New insights into the role of magnetoelastic anisotropy in the magnetization reorientation of magnetic nanowires

D. C. Leitao,[1,*] J. Ventura,[1] C. T. Sousa,[1] A. M. Pereira,[1] J. B. Sousa,[1] M. Vazquez,[2] and J. P. Araujo[1]

[1] *IFIMUP and IN - Institute of Nanoscience and Nanotechnology, Department of Physics and Astronomy, Faculdade de Cincias da Universidade do Porto, Rua do Campo Alegre, 678, 4169-007, Porto, Portugal*

[2] *Instituto de Ciencia de Materiales de Madrid, CSIC Campus Cantoblanco, 28049 Madrid, Spain*

Researchers are focusing intensively on understanding the physical properties of magnetic nanowires (NWs) due to their technological potential. In this work we report a detailed study on the temperature dependence of the magnetic [M(T)] and magneto-transport [MR(T)] properties of Ni and NiFe NWs grown on anodic aluminum oxide (AAO) templates. While the behavior of the NiFe NWs reflected the presence of a strong shape anisotropy, Ni NWs on the other hand showed anomalous M(T) and MR(T). Deviation from the expected M(T) and MR(T) behaviors suggest a reorientation of the magnetization easy-axis with decreasing temperature. We then extracted the temperature variation of the angle between the magnetization and the NWs longitudinal axis, and found an increase from 0° at 370 K to 43° at 5 K. Using a 4th order magnetic anisotropy energy model we were able to successfully explain our results and show that the presence of a magneto-elastic anisotropy contribution due to the compressive stress acting in the NWs is the main origin of the observed magnetization reorientation.

PACS numbers: 73.63.-b, 75.30.Gw, 75.75.-c, 81.07.Gf, 81.15.Pq, 82.45.Cc
Keywords: AAO, magnetic nanowires, magnetoresistance, anisotropy

I. INTRODUCTION

New and interesting phenomena are expected, both from the fundamental and technological points of view, as the geometrical dimensions of magnetic materials become comparable to the electron mean-free-path or the domain-wall width. In particular, systems composed of magnetic nanowires (NWs) with reduced dimensions (few nanometers) can exhibit considerable changes in their physical properties, namely quasi-ideal magnetization (M) reversal processes,[1] quantized-spin-transport[2] or electron localization[3] effects.

Due to the large high-aspect-ratio, one ideally expects magnetic NWs to exhibit a behavior dominated by the strong shape anisotropy and hence a magnetization easy-axis lying along their longitudinal direction. However, when packed in a dense array, a pronounced interplay between the several contributions to the total magnetic anisotropy appears, which can lead to changes in the orientation of the magnetic easy-axis and even to a crossover from the parallel to the perpendicular direction, relatively to the NW long axis.[4,5] By changing the geometrical dimensions (diameter and length)[4,6] or the composition[7,8] of the NWs, one can effectively tune the corresponding magnetic easy-axis orientation.

Arrays of Ni NWs stand as a particular case exhibiting an anomalous magnetic behavior with decreasing temperature (T). Some authors attributed the observed decrease in coercivity and remanence with decreasing T to the irregular surface morphologies of the NWs,[9] while others suggested the presence of a competition between shape and magnetoelastic anisotropies in samples grown either using polycarbonate membranes[10] or anodic aluminum oxide (AAO) templates.[11–13]

Interestingly, a similar behavior was reported for ultrathin Ni films where a spin-reorientation transition (SRT) from in-plane to out-of-plane appeared with decreasing thickness.[14] In this case, the deposition of few monolayers of magnetic material induced drastic changes in the magnetic easy-axis, due to the presence of a strong perpendicular surface anisotropy and enhanced stress.[14–16]

Besides magnetization measurements, electrical and magneto-transport experiments can also give novel insights into magnetic processes in nanostructures. However, and even though the magnetism of ferromagnetic NWs consisting of an interacting dense array or of a single, isolated wire has been exhaustively studied,[6,8,11,13,17,18] few reports can be found on the T-dependence of both electrical resistance [R(T)][19,20] and magnetoresistance [MR(T)].[21,22] Kamalakar et *al.*[20] studied the R(T) behavior of isolated and matrix embedded Ni NWs. They observed a reduced Debye temperature in comparison to bulk Ni and a suppression of the magnetic contribution to R(T) with decreasing NW diameter.[20] This behavior was attributed to the damping of the lattice vibration modes due to the confined dimensionality. In addition, magnetotransport measurements (10 - 300 K) performed in single strands of Ni and NiFe NWs emphasized mainly the identification of magnetization reversal modes.[21,22] Nevertheless, and contrary to what was observed previously using magnetic measurements,[11,13] these transport studies did not report any M-reorientation for AAO embedded Ni NWs.

In this work we report magnetic and magneto-transport measurements performed in arrays of NiFe and Ni NWs embedded in AAO membranes and grown by pulsed electrodeposition. NiFe NWs showed typical M(T) and MR(T) behaviors, translating the presence of

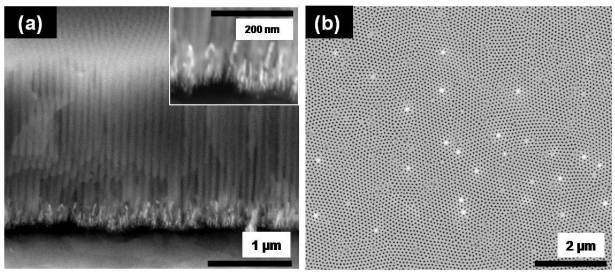

FIG. 1: SEM images of a Cu/NiFe sample: (a) AAO cross-section images with dendrites filled with Cu and (b) top image of Cu/NiFe NWs. Notice that only a small number (0.1 %) of channels is filled.

well defined shape anisotropy. On the other hand, for Ni NWs we obtained a monotonic change of the angle between the magnetization and the NWs longitudinal axis with decreasing temperature. Such behavior is observed independently by M(T) and MR(T) measurements. A 4^{th} order magnetic anisotropy energy model was used to successfully explain our results, showing that the magnetoelastic anisotropy component is the main source for the observed spin reorientation transition.

II. EXPERIMENTAL DETAILS

For the growth of magnetic NWs we used AAO templates obtained by a standard two-step anodization method of high-purity (99.997%) Al foils.[23] After an electropolishing pre-treatment, the Al foils were anodized in a 0.3 M Oxalic acid solution at ∼4°C and under an applied potential of 40 V. The first anodization was carried out for 24 h while the second lasted 1 h. These anodization conditions resulted in nanopores with an average diameter of $\sim$ 35 nm, separation of $\sim$ 105 nm and $\sim$ 2.5 μm in length.

At the bottom of each nanopore, a non-conductive alumina barrier-layer is present, with a nominal thickness that depends on the applied anodization potential.[24] For the conditions used we estimate a barrier-layer of $\sim$ 50 nm. However, for the filling of the nanopores by electrodeposition such insulator layer must be removed or thinned down. Therefore, we reduced the barrier-layer to a nominal thickness of $\sim$ 3 nm, originating dendrites in the process (small channels in the alumina-layer).[25]

The employed procedure retains both the characteristic AAO geometrical features and the underlying Al substrate. Moreover, the barrier-layer thickness is expected to vary slightly from pore to pore, leading to different barrier-layer resistance for each nanopore and consequently to distinctive local deposition rates. A detailed study on the influence of the barrier-layer thickness on the nanopores filling uniformity will be presented elsewhere.[26]

A pulsed electrodeposition method was then used to grow the metallic NWs inside AAO.[25] First, the dendrite channels were filled with Cu from a solution composed of $CuSO_4.5H_20$ and H_3BO_3 [Fig. 1(a)]. The electrodeposition was performed at $\sim$ 303 K with an applied current density of 26 mA/cm^2. The main cylindrical nanopore was subsequently filled with magnetic materials (Ni or NiFe). Further details regarding the corresponding electrodeposition conditions can be found elsewhere.[8] The surface of the samples was then ion-milled, setting the final dimensions of the NWs reaching the surface to 2 μm. Figure 1(b) shows a top-view image of the AAO surface with only a few NWs reaching the top (bright spots). A NW density of $\sim 4 \times 10^7$ NWs/cm^2 is estimated (compare to the AAO template density of $\sim 10^9$ pores/cm^2). Such small filling ratio ($\sim$ 0.1%) is a consequence of the non-uniformity of the alumina barrier thickness and also of the local detachment of the AAO from the underlying Al. Nevertheless, this low NW density allows us to here study the transport properties of a small number of magnetic NWs. The studied samples are thus composed by three distinct segments: the (metallic) magnetic NWs ramify into Cu metallic dendritic channels, which then finish at a $\sim$ 3 nm alumina barrier-layer. The bottom and top electrodes are then the underneath Al foil and a sputter deposited Au thin film, respectively.

The morphology and structure of the samples were studied by Scanning Electron Microscopy (SEM) with a low-vacuum FEI Quanta 400FEG and by X-Ray Diffraction (XRD), using a X'Pert PRO diffractometer in the $\theta - 2\theta$ geometry (Cu-K_α line, λ = 1.5406 Å). M(T) characterization was performed with a Quantum Design SQUID magnetometer, and the R(T) and MR(T) measurements were performed with a pseudo four probe DC method from 20 to 300 K and applied magnetic fields up to 6.5 kOe.

III. EXPERIMENTAL RESULTS

A. Structural Characterization

Figure 2 shows XRD scans for the studied samples. To attain improved details regarding the NWs diffraction patterns, the Al substrate was previously removed. Two main diffraction peaks were observed corresponding to the fcc (111) and (220) structure. A preferential fcc-structure strongly textured along $\langle 110 \rangle$ is present, as typical for template-assisted electrodeposited NWs with high-aspect-ratio.[10,17,27] Using the Scherrer equation and the (220)-peak, we estimate a grain-size (GS) of 100 nm and 30 nm for Ni and NiFe NWs, respectively. Notice that a GS $\sim$ 5 - 20 nm was reported for Ni NWs electrodeposited using a higher current density than the one reported here.[6] The wide bump visible at $\sim 30^\circ$ corresponds to the amorphous alumina from the AAO.

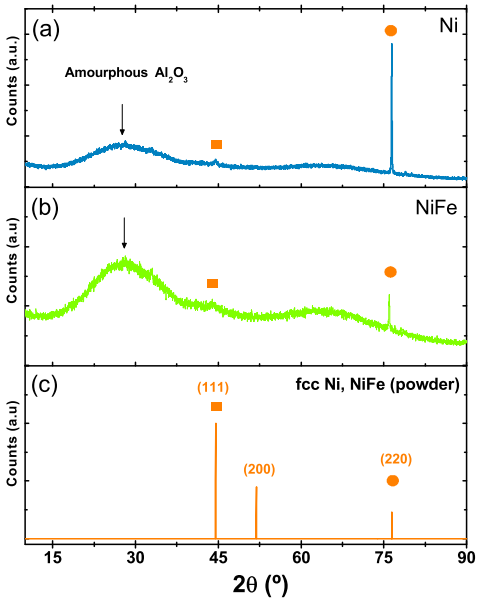

FIG. 2: (color online) $\theta - 2\theta$ XRD scans of (a) Ni, (b) NiFe and (c) corresponding powder diffraction patterns.

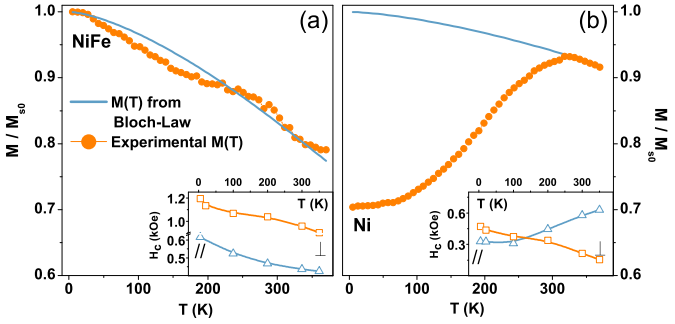

FIG. 3: (color online) Longitudinal M(T) curves of (a) NiFe and (b) Ni NWs. The solid lines represent the expected behavior of M(T) according to Eq. (1). Inset shows H_c(T) for Ni NWs in both configurations; the lines are guides to the eye.

B. Magnetic Properties

Figure 3 shows the field-cooled magnetization versus temperature curves of the NW samples, measured parallel to their longitudinal direction with an applied magnetic field of 50 Oe. For NiFe, one observes the expected growth of the magnetization with decreasing temperature characteristic of a well defined uniaxial anisotropy material [Fig. 3(a)]. In the spin-wave regime (T << T_C), one has:

$$M_s(T) = M_s^0 \left[1 - \beta \left(\frac{T}{T_C}\right)^{3/2}\right], \qquad (1)$$

where T_C is the Curie temperature, M_s^0 the spontaneous magnetization at 0 K [M_s^0(Ni) = 510 emu/cm^3 and M_s^0(NiFe) = 880 emu/cm^3] and the constant β is the fitting parameter.[28] The solid line in Fig. 3(a) displays the theoretical M(T) calculated from Eq. (1), with T_C^{bulk}(NiFe) = 850 K and β = 0.41. The latter was determined from the Arrot plot representation of M(H) curves measured at different temperatures (not shown). Moreover, taking $T_C^{NW} \simeq T_C^{bulk}$ is considered a fair approach, since a significative decrease of T_C in strongly confined systems was reported only for NWs with diameters smaller than 10 nm.[29,30]

On the other hand, the Ni sample displays an anomalous M(T) behavior when compared with NiFe and theoretical expectations [Fig. 3(b)]. In fact, the solid line shows the M(T) calculated using Eq. (1), with T_C^{bulk}(Ni) = 630 K and β = 0.18 (also determined from Arrot plot analyses; not shown). These values are in accordance with previously reported ones.[30] The experimental M(T) data exhibits a slight increase with decreasing temperature [following closely Eq. (1)] down to $\sim$ 330 K. This trend is then followed by a continuous decrease of M(T) down to $\sim 0.7M_s^0$ at 5 K. Such deviation from the expected M(T) behavior indicates that $\vec{M}$ is moving away from the NWs longitudinal axis, pointing towards a reorientation of the magnetization as T decreases,[30,31] as further discussed below.

Interestingly, such behavior is also in accordance with the failure of the thermal activation model in explaining the observed anomalous coercive field [H_c(T)] trend in Ni NWs [inset of Fig. 3(b) for transverse and parallel applied magnetic field].[8] While NiFe shows a continuous increase of H_c(T) with decreasing temperature [inset of Fig. 3(a)][8] characteristic of the dominant shape anisotropy (K_{sh}), the observed H_c(T) for Ni points towards the presence of a weakly defined easy-axis along the NW longitudinal direction.

C. Magnetotransport Properties

The temperature dependent magnetoresistance of the NWs was also studied in detail. First, notice that metallic-like R(T) curves were obtained in both samples, leading us to conclude that the thin alumina-barrier between the dendrites and the Al-foil does not affect considerably our transport measurements [inset of Fig. 4(d)].[32] Such barrier may even be absent, so that the dendritic channels directly contact the Al electrode; in other cases they may be so thin that the resulting resistance is low.

In this work we defined the transverse and parallel MR ($MR^{\perp,//}$) as

$$MR^{\perp,//} = \frac{R^{\perp,//}(H) - R^{\perp,//}(H_{max})}{R^{\perp,//}(H_{max})}, \qquad (2)$$

where $R^{\perp}$ ($R^{//}$) is the resistance measured transverse (parallel) to the electrical current (or equivalently, to the long axis of the NWs), and H_{max} is the maximum applied magnetic field.

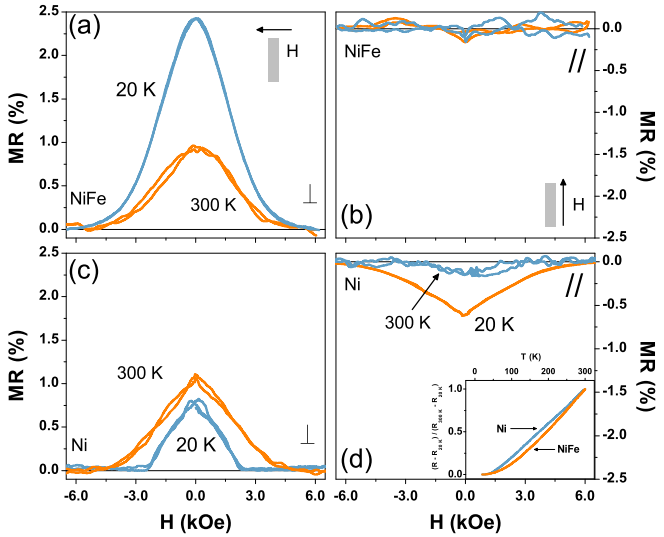

FIG. 4: (color online) Magnetoresistance curves at 300 K and 20 K: (a) $MR^{\perp}$ and (b) $MR^{//}$ for NiFe NWs; (c) $MR^{\perp}$ and (d) $MR^{//}$ for Ni NWs. The inset shows normalized R(T) curves of the NiFe and Ni samples, displaying a metallic-like behavior (dR/dT > 0).

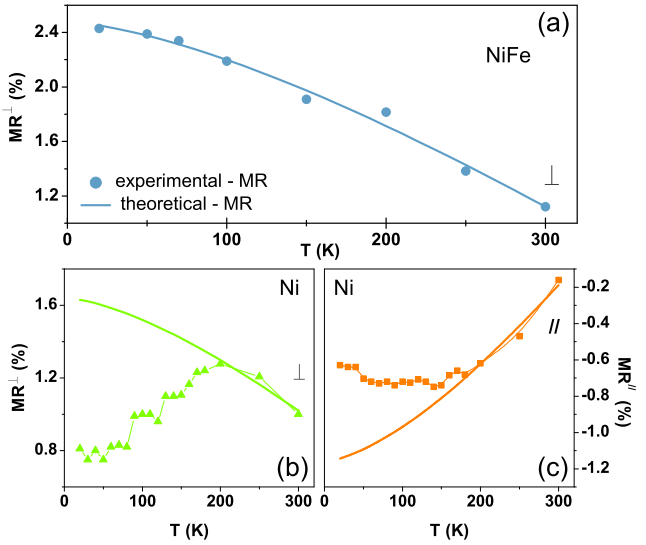

FIG. 5: (color online) Temperature dependence of (a) $MR^{\perp}$ for NiFe, (b) $MR^{\perp}$ and (c) $MR^{//}$ for Ni. The lines are the best fits of Eq. 3 to the experimental data.

Figure 4 displays MR curves for NiFe and Ni NWs at 300 K and 20 K.[33] The bell-shape $MR^{\perp}$ curves display values consistent with those reported in the literature (1 - 1.8% for Ni and 1.2 - 2.4% for NiFe NWs).[21,22] For NiFe NWs we observe the characteristic anisotropic magnetoresistance (AMR) behavior in the considered magnetic field and temperature ranges, with positive $MR^{\perp}$ denoting M-reversal mainly through rotation processes in the transverse geometry, and negligible $MR^{//}_{NiFe}$ values, due to magnetization reversal by domain-wall propagation for H along the longitudinal axis [Fig. 4(b)].

On the other hand, an immediate difference is visible for Ni NWs in the parallel configuration. In fact, a sharper and more triangular $MR^{//}_{Ni}$ curve is observed, together with clearly higher values [$\sim$ 0.8% at 20 K; Fig. 4(d)], again suggesting a magnetic behavior no longer dominated solely by shape anisotropy for Ni NWs.

Figure 5 shows the MR(T) curves for both NW samples. NiFe shows an increase in the MR values with decreasing temperature, resulting from the increase of the spontaneous magnetization and reduction of thermal scattering [Fig. 5(a)]. This MR(T) behavior is characteristic of materials with a well defined uniaxial anisotropy, i.e. a strong M easy-axis. In our case of high-aspect-ratio particles, the presence of a dominant K_{sh} [$K_{sh} = \pi M_s^2(T)$] is expected and was corroborated previously by temperature dependent H_c measurements.[8] On the other hand, Ni NWs initially display an increase in the MR magnitude with decreasing temperature [Figs. 5(b) and (c)], readily followed by a MR decrease.

It is known that M-reversal in NWs takes place mainly by (localized) spin rotation.[1,8,18] One can therefore, in a simple approximation, consider:[34]

$$MR(T) \propto \cos^2[\theta(H,T)] \propto \left[\frac{M_s(T)}{M_s^0}\right]^2, \qquad (3)$$

where θ is the angle between M and the current, which flows along the NW longitudinal direction. The line in Fig. 5(a) shows the fit of the $MR_{NiFe}(T)$ experimental data to Eq. (3), exhibiting a good agreement with the model in the entire T-range. Equation (3) can also be applied to the Ni NWs data, although over a restricted T-range. Only the high temperature data (> 200 K) is within the conditions of dominating K_{sh}, and thus exhibits the usual AMR dependence on temperature. The existence of a significative $MR^{//}$ component in the Ni sample bellow 200 K clearly indicates the onset of a reorientation of the NWs magnetization, away from the long axis direction.

IV. DISCUSSION

A. Spin Reorientation Process

M(T) and MR(T) measurements then allow us to determine the temperature dependence of the angle between M and the NW longitudinal direction [θ_M and θ_{MR}, respectively; Fig. 6(a)]. For the former, one uses $M = M_s^0\cos(\theta)$, while for the latter the sum of the parallel and transverse resistance components has to be taken into account i.e., $R(\theta) = R_{\perp} + (R_{//} - R_{\perp})\cos^2(\theta)$.

A similar θ_M and θ_{MR} behavior is visible, although slight discrepancies appear at high temperatures (> 150 K). This can be attributed to the distinct nature of the

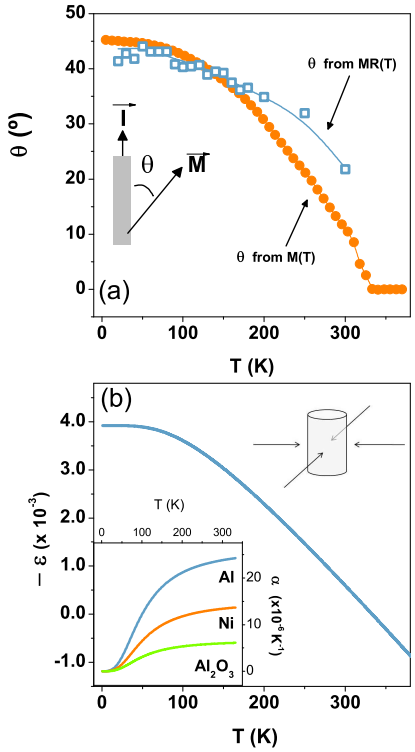

FIG. 6: (color online) (a) θ(T) calculated from M(T) [Fig. 3(b)] and MR(T) [Figs. 5(b) and (c)] measurements; the lines are a guide to the eye. (b) ε(T) obtained from Eq. (4); the inset shows the temperature dependence of $\alpha_{\rm Ni}$, $\alpha_{\rm Al}$ and $\alpha_{\rm Al_2O_3}$ calculated using the Debye model; notice the label $-\varepsilon$ in (b).

experimental methods employed. In fact, while M(T) measurements provide the macroscopic state the magnetization of the sample (long-range order), MR locally probes the degree of alignment between spins within the electron mean-free-path distance (short-range order). Nevertheless, a consistent increase of $\theta_{\rm M,MR}$ with decreasing T is present, reaching $\sim 43^\circ$ at low temperatures.

Noticeably, the magnetization of the NWs should follow Eq. (1) down to the deposition temperature ($T_{\rm dep}$; $\sim$ 303 K). However, one observes that a significant misalignment already exists at 300 K, and that M(T) starts to deviate from Eq. (1) at a higher temperature ($\sim$ 330 K). To explain this fact, one notes that a local temperature rise at the alumina/electrolyte interface during the formation of AAO has been reported.[35] The authors observed a temperature increase between 27 - 35 K for current densities $\sim$ 80 - 200 mA/cm^2, consequence of Joule heating dissipation in the insulator alumina barrier-layer. In analogy, during the electrodeposition process, power dissipation is also expected at the bottom of the nanopores, leading to a localized temperature enhancement. Consequently, an effective (local) deposition temperature $\sim$ 20 - 40 K higher than the electrolyte bath and heating plate can be present during NW growth.

B. Contribution from the Magnetoelastic Anisotropy

Interestingly, a similar MR(T) behavior was reported for a single crystalline free-standing 30 nm Ni NW, and attributed to the temperature dependence of the magnetocrystalline anisotropy ($K_{\rm mc}$).[21] Indeed a spontaneous M reorientation from $\langle 111\rangle$ to $\langle 110\rangle$ crystallographic directions is present in bulk-Ni with decreasing temperature.[39] Notice that, at 300 K, one has the magnetocrystalline anisotropy constants $K_1 = -4.5 \times 10^5$ erg/cm^3 and $K_2 = -0.12 \times 10^5$ erg/cm^3, while at 4.2 K, $K_1 = -0.23 \times 10^5$ erg/cm^3 and $K_2 = 0.3 \times 10^5$ erg/cm^3.[41]

Nevertheless, in polycrystalline and high-aspect-ratio NWs, $K_{\rm sh}$ is significantly large, and is therefore expected to dominate over $K_{\rm mc}$ [$K_{\rm sh}$(300 K) $= 7.2 \times 10^5$ erg/cm^3 and $K_{\rm sh}$(4.2 K) $= 8.1 \times 10^5$ erg/cm^3]. Thus, in our NWs, the presence of a M reorientation should be mediated by another source of anisotropy besides $K_{\rm mc}$. Moreover, previous works on the temperature dependent magnetic properties [M(H,T)] of Ni NWs embedded in AAO reported a pronounced interplay between $K_{\rm sh}$ and the magnetoelastic anisotropy ($K_{\rm me}$).[11–13] Upon cooling, the NWs become subjected to a lateral compressive stress, consequence of the large mismatch between the thermal expansion coefficients (α) of Al, AAO and Ni.[10,11] Contrary to other materials (such as Fe, NiFe, FeCo) where the positive (or null) magnetostriction constant (λ) reinforces $K_{\rm sh}$, in Ni the (large) negative-λ originates a significant magnetoelastic contribution. The result is a weaker effective anisotropy along the NWs longitudinal axis that leads to a reorientation of the magnetization easy-axis towards the transverse direction.[10–13]

Several authors considered as a first approximation a temperature-independent α.[10,11,13] However, and within the framework of the Debye model, α(T) is proportional to the specific heat capacity.[36] The inset of Fig. 6(b) shows α(T) for Ni, Al and Al_2O_3 and, although for T $>$ 200 K α(T) exhibits a fairly linear trend, a tendency towards a constant value is seen as we lower the temperature. The upper limit of the temperature dependent strain [ε(T)] exercised by the Al on the Ni NWs is then given by the mismatch between $\alpha_{\rm Al}$ and $\alpha_{\rm Al_2O_3}$, and can be calculated by:[11,13,37]

$$\varepsilon(\mathrm{T}) = \int_{\mathrm{T_{dep}}}^{\mathrm{T}} [\alpha_{\rm Al_2O_3}(\mathrm{T}) - \alpha_{\rm Al}(\mathrm{T})]\, \mathrm{dT}. \qquad (4)$$

Figure 6(b) displays ε(T) imposed on the NWs by the Al/AAO, considering an effective $T_{\rm dep}$ of 330 K [i. e. ε(330 K) = 0] as inferred from $\theta_{\rm M}$. Remarkably, ε(T) closely resembles the $\theta_{\rm M,MR}$(T) curves obtained from the experimental measurements [Fig. 6(a)], reinforcing the crucial role of $K_{\rm me}$ in the observed reorientation of the magnetization. Notice particularly, the saturation of both ε(T) and $\theta_{\rm M,MR}$(T) below $\sim$ 100 K.

Considering that the NWs are subjected to an in-plane biaxial strain,[38] the axial stress ($\sigma_{\rm ax}$) is then obtained

from:

$$\sigma_{ax} = \frac{\varepsilon(T)}{1-\nu_{Ni}} E_{Ni},$$

with a Poisson coefficient of $\nu_{Ni} = 0.31$ and a Young modulus of $E_{Ni} = 230$ GPa.[11] For 4 K, one estimates $\sigma_{ax} \simeq$ -1.3 GPa ($\sigma_{ax} < 0$ for compression); such a lateral compression, particularly in Ni, will favor an alignment of the magnetization along the contraction axis, i. e. transverse to the longitudinal NW direction.[39] Finally, for ⟨110⟩ textured NWs, the temperature dependent K_{me} term is calculated using $K_{me}(T) = -\frac{3}{2}\lambda_{[110]}\sigma_{ax}$, where $\lambda_{[110]}$ is the bulk saturation magnetostriction constant along ⟨110⟩ ($\lambda_{[110]} = -30.1 \times 10^{-6}$),[40] here taken as constant with temperature.

In fact, at 4 K, a $K_{me} \simeq 5.3 \times 10^5$ erg/cm^3 is obtained, of the same order of K_{sh}. This competition between K_{sh} and K_{me} qualitatively explains the reorientation of the magnetization easy-axis.

C. Phenomenological Energy Model

To further clarify the nature of the observed SRT and in analogy to the in-plane to out-of-plane SRTs observed in ultrathin magnetic films,[15] we resort to a simple magnetic anisotropy energy model. To allow the presence of a monotonic rotation of the magnetization, one must take into consideration higher order terms in the total energy of the system [E(T, θ)].[14] A 4th order expansion of E(T, θ) enables the existence of stable θ values between 0 and 90°, thus portraying the continuous nature of our temperature driven SRT. The energy of the system is then given by (neglecting in-plane variations):

$$E(T,\theta) = K_2^{eff}(T)\,\sin^2(\theta) + K_4^{eff}(T)\,\sin^4(\theta). \qquad (5)$$

In the above equation, the 2nd order effective anisotropy constant (K_2^{eff}) comprehends all the (2nd order) magnetostatic terms, namely shape and macroscopic demagnetizing anisotropies (K_{sh} and K_{md}, respectively), and the magnetoelastic anisotropy (K_{me}). K_{md} represents the anisotropy originating from the macroscopic demagnetizing field of the whole sample given by $K_{md} = 4\pi M_s P$, where P is the sample porosity (usually $\sim$ 10 % for a completely filled AAO).[6] For a cubic system, K_{mc} should appear only on 4th order terms [$K_4^{eff}(T)$] in addition to higher-order magnetoelastic terms and other possible sources of anisotropy.[42] For a continuous transition to occur [such as the one seen in Fig. 6(a)], this model requires $K_2^{eff}(T) < 0$ and $K_4^{eff}(T) > 0$ during the SRT.

In fact, and within this framework, the decrease of $H_c^{//}$ with decreasing T [inset of Fig. 3(b)] also supports a $K_2^{eff} < 0$; the latter leads to the weakly defined M easy-axis along the NWs long direction, which in turn translates into lower H_c values. Moreover, a crossover between $H_c^{//}$ and $H_c^{\perp}$ is visible below $\sim$ 150 K, from whereon small differences are observed between both H_c

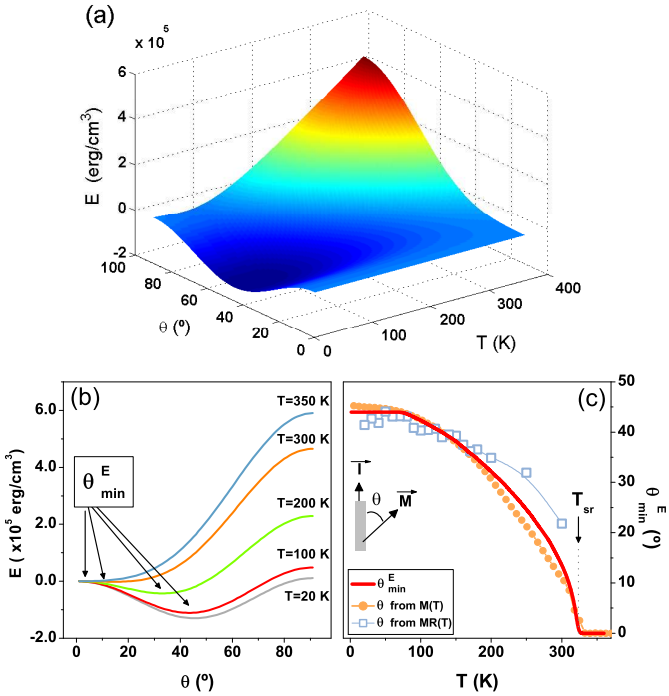

FIG. 7: (color online) (a) Energy map for the Ni NWs system obtained from Eq. (5). (b) E(θ) curves for selected temperatures obtained from (a) and stressing the presence of a minimum angle at lower temperatures. (c) Comparison between θ^E_{min} obtained from E(T, θ) minimization to the experimental $\theta_{M,MR}$.

values. Such characteristic is in turn coincident with the saturation feature observed in both θ(T) and ε(T) (Fig. 6). c Figure 7(a) displays the E(T, θ) color map for our Ni NWs system, calculated using the already computed anisotropy values, considering a K_{sh}-value corrected for multidomain NWs (see below). A continuous variation with T of the energy minimum is visible, with an absolute minimum $\sim$ 43° at low temperatures [< 50 K; Fig. 7(b)]. The T-dependent angle (between M and the NW long axis) corresponding to the minimum of E(T, θ) [θ^E_{min}] is shown in Fig. 7(c). Notice that θ^E_{min}(T), giving the stable canted magnetization state, follows the same trend as the experimentally obtained $\theta_{M,MR}$(T), mainly retaining the shape of ε(T).

The best correlation of θ^E_{min} with our experimental results was obtained for a K_{sh} 60 - 75 % smaller than theoretically expected. In fact, the presence of local anisotropies arising from defects and finite dimensions lead to a decrease of the total anisotropy in NW systems, resulting in a multidomain structured NWs,[43–45] and thus lower H_c values and localized magnetization reversal.[8,46,47]

Moreover, considering that such an accentuated decrease in K_{sh} is indeed reflecting a decrease in the form factor (N=1/2 for infinite long NWs), one obtains an effective NWs monodomain length of $\sim$ 47 nm. We high-

light that such a value is in accordance with theoretical results, which consider the NWs as a magnetostatically-coupled chain of ellipsoids with a monodomain size of $\sim$ 20 - 30 nm.[45,48]

V. CONCLUSIONS

We presented a thorough study of the M(T) and MR(T) behaviors in a temperature range between 5 and 370 K, for Ni and NiFe NWs with $\sim$ 35 nm diameter and $\sim$ 2 μm in length. The NiFe samples revealed the usual magnetic and transport behavior with temperature, consistent with dominant shape anisotropy. In contrast, we established a continuous rotation of the magnetization for Ni NWs from both M(T) and MR(T) measurements. Due to the polycrystalline nature of our NWs, the origin of such anomalous phenomena required an additional source of anisotropy besides K_{mc}. The presence of a strong K_{me} contribution (perpendicular to the NW) was suggested, consequence of the large mismatch between thermal expansion coefficients. Moreover, the continuous spin reorientation transition is successfully described using a 4^{th} order expansion of the energy of the system, considering effective anisotropy constants. The modeled angle between the magnetization and the NW axis showed a remarkable agreement with the experimental results, suggesting at the same time the presence of multidomain NWs with an average monodomain size of $\sim$ 47 nm.

Acknowledgments

Work supported in part by project FEDER/POCTI/n2-155/94. D. C. Leitao, C. T. Sousa and A. M. Pereira are thankful for FCT grants (SFRH/BD/25536/2005, SFRH/BD/38290/2007, SFRH/BPD/63150/2009). J. Ventura acknowledges funding through FSE/POPH. J.P. Araujo also thanks Fundação Gulbenkian for its financial support within the "Programa Gulbenkian de Estímulo a Investigação Científica".

* Electronic address: dleitao@fc.up.pt

[1] W. Wernsdorfer, B. Doudin, D. Mailly, K. Hasselbach, A. Benoit, J. Meier, J. P. Ansermet, and B. Barbara, Phys. Rev. Lett. **77**, 1873 (1996).
[2] F. Elhoussine, S. Matefi-Tempfli, A. Encinas, and L. Piraux, Appl. Phys. Lett. **81**, 1681 (2002).
[3] D. Neumaier, A. Vogl, J. Eroms, and D. Weiss, Phys. Rev. B **78**, 174424 (2008).
[4] M. Vazquez, K. Pirota, M. Hernandez-Velez, V. M. Prida, D. Navas, R. Sanz, F. Batallan, and J. Velazquez, J. Appl. Phys. **95**, 6642 (2004).
[5] J. Escrig, R. Lavin, J. L. Palma, J. C. Denardin, D. Altbir, A. Cortes, and H. Gomez, Nanotech. **19**, 075713 (2008).
[6] K. Nielsch, R. B. Wehrspohn, J. Barthel, J. Kirschner, U. Gosele, S. F. Fischer, and H. Kronmuller, Appl. Phys. Lett. **79**, 1360 (2001).
[7] L.-P. Carignan, C. Lacroix, A. Ouimet, M. Ciureanu, A. Yelon, and D. Menard, J. Appl. Phys. **102**, 023905 (2007).
[8] D. C. Leitao, C. T. Sousa, J. Ventura, K. R. Pirota, M. Vazquez, J. B. Sousa, and J. P. Araujo, J. Mag. Magn. Mat. **322**, 1319 (2010).
[9] H. Zeng, S. Michalski, R. D. Kirby, D. J. Sellmyer, L. Menon, and S. Bandyopadhyay, J. Phys. - Cond. Matt. **14**, 715 (2002).
[10] S. Pignard, G. Goglio, A. Radulescu, L. Piraux, S. Dubois, A. Declemy, and J. L. Duvail, J. Appl. Phys. **87**, 824 (2000).
[11] A. Kumar, S. Fahler, H. Schlorb, K. Leistner, and L. Schultz, Phys. Rev. B **73**, 064421 (2006).
[12] J. Sanchez-Barriga, M. Lucas, F. Radu, E. Martin, M. Multigner, P. Marin, A. Hernando, and G. Rivero, Phys. Rev. B **80**, 184424 (2009).
[13] D. Navas, K. R. Pirota, P. M. Zelis, D. Velazquez, C. A. Ross, and M. Vazquez, J. Appl. Phys. **103**, 07D523 (2008).
[14] M. Farle, B. Mirwald-Schulz, A. N. Anisimov, W. Platow, and K. Baberschke, Phys Rev B **55**, 3708 (1997), and references therein.
[15] B. Schulz and K. Baberschke, Phys. Rev. B **50**, 13467 (1994), and references therein.
[16] I. Yamamoto, T. Nakagawa, Y. Takagi, and T. Yokoyama, Phys. Rev. B **81**, 214442 (2010).
[17] Q. Zhan, Z. Chen, D. Xue, F. Li, H. Kunkel, X. Zhou, R. Roshko, and G. Williams, Phys. Rev. B **66**, 134436 (2002).
[18] H. Zeng, R. Skomski, L. Menon, Y. Liu, S. Bandyopadhyay, and D. J. Sellmyer, Phys. Rev. B **65**, 134426 (2002).
[19] M. V. Kamalakar, A. K. Raychaudhuri, X. Wei, J. Teng, and P. D. Prewett, Appl. Phys. Lett. **95**, 013112 (2009).
[20] M. V. Kamalakar and A. K. Raychaudhuri, Phys. Rev. B **79**, 205417 (2009).
[21] Y. Rheem, B. Y. Yoo, W. P. Beyermann, and N. V. Myung, Nanotech. **18**, 015202 (2007).
[22] Y. Rheem, B. Y. Yoo, B. K. Koo, W. P. Beyermann, and N. V. Myung, J. Phys. D: Appl. Phys. **40**, 7267 (2007).
[23] H. Masuda and K. Fukuda, Science **268**, 1466 (1995).
[24] K. Nielsch, J. Choi, K. Schwirn, R. B. Wehrspohn, and U. Gosele, Nano Lett. **2**, 677 (2002).
[25] K. Nielsch, F. Muller, A. P. Li, and U. Gosele, Adv. Mater. **12**, 582 (2000).
[26] C. T. Sousa, D. C. Leitao, M. P. Proenca, A. Apolinario, J. G. Correia, J. Ventura, and J. P. Araujo, to be published.
[27] F. Maurer, J. Brotz, S. Karim, M. Eugenia, T. Molares, C. Trautmann, and H. Fuess, Nanotech. **18**, 135709 (2007).
[28] C. A. F. Vaz, J. A. C. Bland, and G. Lauhoff, Rep. Prog. Phys. **71**, 056501 (2008).
[29] D. Zhang, K. J. Klabunde, C. M. Sorensen, and G. C. Hadjipanayis, Phys. Rev. B **58**, 14167 (1998).
[30] M. Zheng, L. Menon, H. Zeng, Y. Liu, S. Bandyopadhyay, R. D. Kirby, and D. J. Sellmyer, Phys. Rev. B **62**, 12282 (2000).

[31] A. M. Pereira, J. B. Sousa, J. P. Araujo, C. Magen, P. A. Algarabel, L. Morellon, C. Marquina, and M. R. Ibarra, Phys. Rev. B **77**, 134404 (2008).

[32] D. C. Leitao, C. T. Sousa, J. Ventura, J. S. Amaral, F. Carpinteiro, K. R. Pirota, M. Vazquez, J. B. Sousa, and J. P. Araujo, J. Non-Cryst. Sol. **354**, 5241 (2008).

[33] No discontinuous jumps in the $MR^{\perp,//}$ curves are observed, consequence of measuring several NWs in parallel. Also, for a parallel array of N equivalent NWs, the MR ratio is given by $\frac{1}{N}\sum_N \left[\frac{\Delta R_{nw}}{R_{nw}}\right] \simeq MR_{nw}$, i.e. nearly independent of the number of NWs.

[34] J. E. Wegrowe, D. Kelly, A. Franck, S. E. Gilbert, and J. P. Ansermet, Phys. Rev. Lett. **82**, 3681 (1999).

[35] I. De Graeve, H. Terryn, and G. E. Thompson, J. Appl. Electrochem. **32**, 73 (2002).

[36] C. Kittel, *Introduction to Solid State Physics* (Wiley, 1996), 7th ed.

[37] S. Kato, H. Kitazawa, and G. Kido, J. Mag. Magn. Mat. **272-276**, 1666 (2004).

[38] D. Navas, C. Nam, D. Velazquez, and C. A. Ross, Phys. Rev. B **81**, 224439 (2010).

[39] R. M. Bozorth, *Ferromagnetism* (IEEE Press, 1951).

[40] S. Chikazumi, *Physics of Magnetism* (Wiley, 1959).

[41] M. Hwang, M. Shima, C. A. Ross, C. Seberino, and H. N. Bertram, J. Appl. Phys. **92**, 1018 (2002).

[42] M. Jamet, W. Wernsdorfer, C. Thirion, D. Mailly, V. Dupuis, P. Melinon, and A. Perez, Phys. Rev. Lett. **86**, 4676 (2001).

[43] Y. Henry, A. Iovan, J. M. George, and L. Piraux, Phys Rev B **66**, 184430 (2002).

[44] L. Guirado, oacute, R. A. pez, J. M. Montejano-Carrizalez, Mor, aacute, L. n, and J. L. pez, Phys Rev B **77**, 134431 (2008).

[45] X. Lu, S. Ge, L. Jiang, and X. Wang, J Appl Phys **97**, 084304 (2005).

[46] P. M. Paulus, F. Luis, M. Kroll, G. Schmid, and L. J. de Jongh, J. Mag. Magn. Mat. **224**, 180 (2001).

[47] H. B. Braun, Phys. Rev. Lett. **71**, 3557 (1993).

[48] F. Tian, J. Chen, J. Zhu, and D. Wei, J Appl Phys **103**, 013901 (2008).